Planar bifunctional Luneburg-fisheye lens made of an anisotropic metasurface

Wan, Xiang; Shen, Xiaopeng; Luo, Yu; Cui, Tie Jun

2014

Wan, X., Shen, X., Luo, Y., & Cui, T. J. (2014). Planar bifunctional Luneburg-fisheye lens made of an anisotropic metasurface. Laser & Photonics Reviews, 8(5), 757-765.

https://hdl.handle.net/10356/83827

https://doi.org/10.1002/lpor.201400023

Planar Bi-Functional Luneburg-Fisheye Lens Made of Anisotropic Metasurface

Xiang Wan[1], Xiaopeng Shen[1], Yu Luo[2*], and Tie Jun Cui[1*]

[1]*State Key Laboratory of Millimetre Waves, School of Information Science and Engineering, Southeast University, Nanjing 210096, China.*

[2] *Imperial College London, Department of Physics, The Blackett Laboratory, London SW7 2AZ, UK.*

[*] *Email: luoyu@ntu.edu.sg; tjcui@seu.edu.cn*

Luneburg lens and Maxwell fisheye lens are well-known microwave and optical devices with distinct focusing properties. Here, we present a planar bi-functional Luneburg-fisheye lens made of anisotropic metasurface, which features as Luneburg along the horizontal optical axis while as fisheye along the vertical optical axis. We propose a method to control the inhomogeneous indexes of refraction independently along the two optical axes by designing anisotropic and non-uniform metasurface, which can provide the required distributions of refractive indexes approximately for Luneburg and fisheye lenses watching from the two optical axes. Experiments in the microwave frequency demonstrate very good performance of the planar bi-functional Luneburg-fisheye lens. The proposed method opens a venue to design other kinds of bi-functional devices using metasurfaces in the microwave, terahertz, and even optical frequencies.

Keywords: Bi-functional device, planar Luneburg-fisheye lens, metasurface, anisotropic

1. Introduction

In the classical physics, Luneburg lens and Maxwell fisheye lens are two typical optical devices with the spherical symmetry. The Luneburg lens, whose index of refraction (n) is gradually changed in the sphere and satisfies $n=\sqrt{2-(r/R)^2}$ (R is the radius of sphere), can make the image of a point source on the lens surface to an infinite distance in the opposite direction [1]; while the Maxwell fisheye lens is an ultra- wide-angle lens with $n=n_0/[1+(r/R)^2]$ (n_0 is the maximum index of refraction at the lens center), which makes the image of a point source on the lens surface to the opposite point on the surface [2]. Both Luneburg and fisheye lenses have important applications in the optical and microwave frequencies, such as collimating lights, radar antennas, and wide-angle cameras. Now a raised question is: Can we integrate the Luneburg lens and fisheye lens together? That is to say, can we make a single lens to serve as either Luneburg or fisheye? The answer is: it is possible by using anisotropic materials to control the refractive indexes along the two optical axes. However, it is extremely difficult to perform this task using natural materials due to the distinctly inhomogeneous refractive-index distributions of Luneburg and fisheye lenses. The emerging metamaterials [3-6] may provide a possibility to solve the problem.

Metamaterials are artificial periodic or quasi-periodic structures with unit cells in subwavelength scales, which can be engineered to achieve unusual effective medium parameters (the electric permittivity ε, magnetic permeability μ, and refractive index n) beyond the natural existence, such as negative or zero index of refraction. Under the guidance of transformation optics [7,8], metamaterials have demonstrated a series of fantastic physical phenomena, including the negative refraction [6], invisibility cloaks [9-18], flatted Luneburg lenses [19,20], optical illusions [21,22], and the optical ‘‘Janus’’ device [23]. Nevertheless, the experimental verifications to such transformation-optics devices are still limited owing to the requirements of inhomogeneous and anisotropic material parameters. Currently, the available experiments have mainly been focused

on the weakly anisotropic (or nearly isotropic) inhomogeneous devices [12-15,19,20,23], strongly anisotropic but homogeneous carpet cloak [17,18], and simplified-parameter invisibility cloak [9] and optical-illusion devices [22] that have only one-directional variation of anisotropic material parameters.

Recently, a special version of metamaterials, metasurfaces with gradient phase changes, has received great interests due to their outstanding features, planar geometries, and easy fabrications [24-33]. By introducing periodically gradient phase shifts from 0 to 2π along one direction on a metasurface, which are generated from differently-oriented V-shaped nano antennas, anomalous reflections and refractions governed by the Fermat principle have been observed when the electromagnetic waves are passing through the metasurface [24]. Inspired by the generalized Snell's laws of reflection and refraction, the gradient-phase metasurfaces have been applied in constructing optical vortex [24,25], broadband light bending [26], photonic spin Hall effect [27], polarization traffic control [28,29], and the polarization rotations [30]. Other-shaped nano antennas have also been proposed to realize a dual-polarity plasmonic lens for circularly-polarized lights with different rotations [31] and to convert the propagating waves to surface plasmons efficiently [32,33]. All these unusual features [24-33] are based on the gradient-phase variations along one direction.

From above discussions, we notice that the current designs of bulk metamaterials and planar metasurfaces are still difficult to control anisotropic and inhomogeneous distributions of material parameters independently along two optical axes. Here, we propose a method to design two distinct inhomogeneous indexes of refraction along the two optical axes of anisotropic metasurface. U-shaped particles are introduced to realize the anisotropic metasurface with varied anisotropy from weak to strong. Based on the proposed method and U-shaped particles, a bi-functional Luneburg-fisheye planar lens is presented, which performs like a Luneburg lens along the horizontal optical axis while like a fisheye lens along the vertical optical axis. Experiments in the microwave frequency validate the bi-functional features.

We remark that proposed bi-functional device is significantly different from the earlier designed optical "Janus" device[23], which is based on the transformation optics

(exactly, the quasi-conformal mapping) and whose refractive index is everywhere isotropic. When illuminated in different directions, the optical "Janus" device acts like a lens and a beam shifter correspondingly [23]. Advantages of the proposed anisotropic bi-functional design can be summarized as follows. 1) The anisotropy-based design is more flexible and can be easily used to realize other bi-functional devices, such as Luneburg-Eaton lens, Eaton-fisheye lens, etc. 2) It deploys the metasurface concept, and the bi-functional device is a planer and single-layer structure. Compared with the bulk device [23], the planer structure is more suitable for integrations. 3) From the viewpoint of materials, we propose a method to design and realize anisotropic and inhomogeneous material properties in two orthogonal directions, which is difficult for earlier bulk metamaterials [3-23] and metasurfaces [24-33].

2. Design, numerical simulations, and experiments

We start by considering an anisotropic metasurface that is composed of two-dimensional (2D) periodic subwavelength particles. We introduce a metallic U-shaped structure on the dielectric slab as unit cell of the anisotropic metasurface, as shown in Fig. 1 and the inset of Fig. 2(b). A single U-shaped particle has an electric dipole moment $\boldsymbol{P}$ along the horizontal direction and a magnetic dipole moment $\boldsymbol{M}$ along the vertical direction [34]. Hence the particle will mainly interact with the horizontal component of the electric field and the vertical component of the magnetic field, which corresponds to the transverse-electric (TE)-mode surface waves on the metasurface. Usually, the array of U-shaped particles together with the dielectric slab can be treated as an impedance surface with capacitive surface impedance. However, this equivalent treatment suffers from the spatial dispersion constraint, i.e., the working frequency of the metasurface should be chosen to avoid being close to the boundary of the first Brillouin zone. Otherwise, the Magneto-inductive waves [35] may emerge due to strong magnetic couplings between the U-shaped particles. The important advantage to use the U-shaped particle is the freedom to control anisotropy of metasurface by changing the groove depth h (see Fig. 1), and the anisotropic

manipulation mainly relies on the anisotropic electric resonances. This can be understood by considering the components of the Poynting vector **S**. For the TE-mode surface waves, we have $\overline{\overline{\mathbf{S}}} = E_y H_z \hat{x} + E_x H_z \hat{y}$, indicating that the anisotropic electric resonance will lead to anisotropic propagating properties of surface waves.

The detailed U-shaped structure is demonstrated in Fig. 1, in which an ultrathin U-shaped metallic film is printed on a supporting dielectric slab. The size of the dielectric slab is $p_x \times p_y$, which is also the period of the particle array, with the thickness t. The size of the metallic patch is $d_x \times d_y$, and the groove width and depth are w and h, respectively. The designed values of such parameters are given in the caption of Fig. 1. Based on the commercial software, CST Microwave Studio, the 2D dispersion surface of the metasurface is obtained under such a design, which describes the relations among the frequency and wave numbers in the x and y directions (k_x and k_y), as demonstrated in Fig. 2(a). From the simulation results of iso-frequency curves shown in Fig. 2(b), we observe that the degree of anisotropy is relatively strong when h is large, while the particle tends to be isotropic when h is small. In particular, at the frequency of 10 GHz, we have k_x=417 and k_y=294 (strong anisotropy) when h=3.4 mm; while k_x=247 and k_y=247 (isotropy) as h=1 mm. According to the relation between wavenumber and refractive index, we obtain the surface indexes of refraction along the x and y directions as $n_x = k_x / k_0$ and $n_y = k_y / k_0$, in which k_0 is the free-space wavenumber. Hence the surface refractive indexes of the anisotropic metasurface can be tailored by adjusting the groove depth h.

Next we consider a 2D array of the U-shaped particles which are either homogeneous or inhomogeneous, as shown in Fig. 2(c), in which x and y are two optical axes and a point source is located on the horizontal optical axis. If the electromagnetic ray emitting from the point source is parallel to the x axis, the surface refractive index is denoted as $n_{xx}=n_x$ (see Particle A); if the ray is parallel to the y axis, the surface refractive index is denoted as $n_{yy}=n_y$. Hence the refractive index tensor on the anisotropic metasurface can be written as $\overline{\overline{\mathbf{n}}}_s = n_{xx}\hat{x}\hat{x} + n_{yy}\hat{y}\hat{y}$. When the ray is incident to a particle at an oblique angle θ with respect to the x axis (see Particle B),

then we rotate the *x*-*y* axes counter-clockwise by the angle of θ to form new *x*'-*y*' axes so that the ray is parallel to the *x*' axis locally, as illustrated in Particle B. In the new coordinate system (*x*', *y*'), the refractive index tensor is given by a coordinate transformation: $\overline{\overline{\mathbf{n}}}'_s = \overline{\overline{\mathbf{R}}}_\theta^{\mathrm{T}} \cdot \overline{\overline{\mathbf{n}}}_s \cdot \overline{\overline{\mathbf{R}}}_\theta$, in which $\overline{\overline{\mathbf{R}}}_\theta = \hat{x}\hat{x}\cos\theta - (\hat{x}\hat{y} - \hat{y}\hat{x})\sin\theta + \hat{y}\hat{y}\cos\theta$ is the transformation dyadic. After simple calculations, the explicit expression of $\overline{\overline{\mathbf{n}}}'_s$ is derived as

$$n'_{xx} = n_{xx}\cos^2\theta + n_{yy}\sin^2\theta, \quad n'_{yy} = n_{xx}\sin^2\theta + n_{yy}\cos^2\theta,$$
$$n'_{xy} = n'_{yx} = -(n_{xx} - n_{yy})\sin\theta\cos\theta. \tag{1}$$

From above equations, we clearly notice that cross couplings exist and the refractive index tensor is highly anisotropic. To eliminate the cross couplings, an easy way is letting n_{xx}=n_{yy}, which corresponds to *h*=1 mm in the U-shaped particle. Then we have n'_{xy}=n'_{yx} and n'_{xx}=n'_{yy}, and hence the metasurface is purely isotropic.

However, we here require the metasurface to be anisotropic along the *x* and *y* optical axes; while along each optical axis, we hope the metasurface to be nearly isotropic for different incident angles to realize the bi-functional devices. From Eq. (1), when θ is small, we will obtain $n'_{xx} \approx n_{xx}$, $n'_{yy} \approx n_{yy}$, and $n'_{xy} \approx n'_{yx} \approx 0$, in which n_{xx} and n_{yy} can be significantly different. As θ is large, we can also obtain $n'_{xx} \approx n_{xx}$, $n'_{yy} \approx n_{yy}$, and $n'_{xy} \approx n'_{yx} \approx 0$ by forcing n_{xx} and n_{yy} to be identical approximately. That is to say, in order to keep isotropy of metasurface by observing from one optical axis, the deviation between n_{xx} and n_{yy} can be significant for particles with small incidence angles; for particles with large incidence angles, however, the deviation has to be small. Therefore, if we design the metasurface with strongly anisotropic particles (deep grooves) in the region where the ray direction is nearly parallel to the optical axis, and with weakly anisotropic particles (shallow grooves) in the region where the ray direction deviates from the optical axis, we can separate the principle components of the tensor index of refraction approximately. As a result, we

can design the anisotropic and inhomogeneous metasurface in different optical axes nearly independently in a way similar to the isotropic metasurface.

Now we apply for the above method to design an anisotropic metasurface which performs like the Luneburg lens in the horizontal optical axis and the Maxwell fisheye lens in the vertical optical axis. Fig. 3(a) illustrates the schematic of the anisotropic metasurface. We should calculate the groove depths (h) appropriately to obtain the required n_x for Luneburg lens (see Fig. 3(b)) and the required n_y for fisheye lens (see Fig. 3(c)). Since the surface refractive indexes of Luneburg and fisheye lenses are rotationally symmetric, the distribution of h on the metasurface can be written in the form as

$$h(r) = -\frac{(h_{max} - h_{min})}{e^{tR} - 1} e^{tr} + \frac{h_{max} e^{tR} - h_{min}}{e^{tR} - 1},$$

where h_{max} and h_{min} are the largest and smallest depths of grooves, R is the radius of the bi-functional metalens, and t is a fitting factor. From full-wave simulations, we obtain the fitting factor as t=0.09 to ensure the requirements of Luneburg (Fig. 3(b)) and fisheye (Fig. 3(c)) lenses simultaneously. Fig. 3(d) illustrates the calculation results of the effective indexes of refraction along the two optical axes of the bi-functional metalens using the fitting groove depths, which are very close to the ideal refractive-index distributions of Luneburg and fisheye lenses (solid lines). We notice that small offsets exist between the effective parameters and ideal values due to the fitting error, but they make small influence to the performance of the bi-functional device, as shown later.

To validate the concept and performance of the bi-functional Luneburg-fisheye metasurface lens, we conduct full-wave simulations to the designed structure (see Fig. 3(a)) in the microwave frequency (10 GHz), and the numerical results of electric fields are demonstrated in Figs. 4(a), (b), (d), and (e). When an electric dipole is placed at the leftmost of the lens, the near electric fields on an observation plane that is 1 mm above the metasurface are presented in Fig. 4(a). We clearly observe that the spherical waves radiated from the dipole source are converted to plane waves by the

metasurface, representing the main physics of a Luneburg lens, as predicted in Fig. 3(b). However, when the electric dipole is placed at the bottom of the lens, the simulation results (Fig. 4(d)) show that the same metasurface will focus the point source on the opposite position of the metalens, as predicted by the ray-tracing strategy (Fig. 3(c)). Apparently, the designed anisotropic metasurface does realize the bi-functional features of Luneburg lens and fisheye lens. The field distributions on the vertical observation planes passing the two optical axes are given in Figs. 4(b) and 4(e), which show the nature of surface plasmons, i.e., the fields decay exponentially on two sides of the metasurface within the lens. Fig. 5 demonstrates the quantitative field distributions along the z direction (i.e., perpendicular to metasurface) on the horizontal and vertical optical axes. In both cases, we observe exponential decays of fields on two sides of the metasurface, illustrating excellent localization performance.

Besides the co-polarized electric fields, we have also simulated the cross-polarized electric fields for the Luneburg lens (E_y) and Maxwell fisheye lens (E_x), as illustrated in Figs. 6(a) and (b), respectively. For the TE-mode surface waves, the Poynting vector is expressed as $\overline{\overline{\boldsymbol{S}}} = \boldsymbol{E}_y \boldsymbol{H}_z \hat{x} + \boldsymbol{E}_x \boldsymbol{H}_z \hat{y}$. Since the Luneburg lens is designed along the y direction by modulating k_y, the electric field E_x is dominant. Similarly, the fisheye lens is designed along the x direction, and hence E_y is dominant. The cross-polarized electric fields nearly do not affect the power flows of the Luneburg and fisheye lenses, as shown in Figs. 6(c) and (d).

We fabricate the designed sample, as shown in Figs. 7(a) and (b), and measure it in the microwave frequency. Similar to the case of simulations, an electric dipole (see Fig. 7(c)) is used as the excitation source on the two optical axes. Another electric dipole with the same polarization serves to detect the electric fields on the observation plane that is 1 mm above the metasurface. In measurements, the fabricated sample of the bi-functional metasurface lens is fixed on an operation platform, which can move in both x and y directions, controlled by the motion controller to achieve automated near-electric field scanning with resolution of 1 mm, as demonstrated in Fig. 8. The excitation and detecting electric dipoles with the same polarization are connected to

an Agilent N5230C network analyzer using the coaxial lines. When the source is excited on the horizontal and vertical optical axes, the measured results are illustrated in Figs. 4(c) and (f), respectively, which have very good agreements to the full-wave simulations given in Figs. 4(a) and (d), showing excellent performance of the planar bi-functional Luneburg-fisheye metalens.

3. Summary

We have proposed a method to control the inhomogeneous refractive indexes independently along two optical axes by designing the anisotropic and non-uniform metasurface. Based on this method, we obtained the distributions of refractive indexes for the Luneburg lens and fisheye lens watching from the two optical axes of a single metasurface. Hence, we have presented a planar bi-functional Luneburg-fisheye lens, which features as Luneburg along the horizontal optical axis while as fisheye along the vertical optical axis. Numerical simulations and experiments have shown very good performance of the planar bi-functional device. Although our design and demonstration on the bi-functional Luneburg-fisheye lens are conducted in the microwave frequency, they can be directly extended to the terahertz frequency and may be extended to infrared and optical regimes. Due to the ability to tailor the inhomogeneous indexes of refraction on two optical axes independently, the proposed method provides a way to realize other kinds of bi-functional metasurface devices. We remark that the proposed planar bi-functional device and designing method are totally different from the earlier optical "Janus" device based on quassi-conformal mapping [23] and other transformation-optics devices with different functionalities to different-polarized waves (only simulations) [36,37].

Acknowledgements.

X. W. and T. J. C. contributed equally to this work. The work was supported in part by the National High Tech (863) Projects (2012AA030402 and 2011AA010202), in

part by the National Science Foundation of China (60990320, 60990324 and 61138001), and in part by the 111 Project (111-2-05).

References

1. Luneburg, R. K., *Mathematical Theory of Optics* (Brown Univ. Press, Providence, Rhode Island, 1944).

2. Maxwell, J. C., *The Scientific Papers of James Clerk Maxwell*, Niven, W. D., ed. (Dover, New York, 1890).

3. Cui, T. J., Smith, D. R. & Liu, R., eds., *Metamaterials – Theory, Design, and Applications* (Springer, New, York, 2009).

4. Pendry, J. B., Holden, A. J. & Stewart, W. J., Extremely low frequency plasmons in metallic mesostructures. *Phys. Rev. Lett.* **76,** 4773 (1996).

5. Pendry, J. B., Holden, A. J., Robbins, D. J. & Stewart, W. J., Magnetism from conductors and enhanced nonlinear phenomena. *IEEE Trans. Micro. Theory Tech*. **47,** 2075 (1999).

6. Shelby, R. A., Smith, D. R. & Schultz, S., Experimental verification of a negative index of refraction. *Science* **292,** 77 (2001).

7. Pendry, J. B., Shurig, D. & Smith, D. R., Controlling electromagnetic fields. *Science* **312,** 1780 (2006).

8. Leonhardt, U., Optical conformal mapping. *Science* **312,** 1777 (2006).

9. Schurig, D. *et al.*, Metamaterials electromagnetic cloak at microwave frequencies. *Science* **314,** 977(2006).

10. Cai, W., Chettiar U. K., Kildishev, A. V. & Shalaev, V. M., Optical cloaking with metamaterials. *Nat. Photon*. **1,** 224 (2007).

11. Li, J. & Pendry, J. B., Hiding under the carpet: a new strategy for cloaking. *Phys. Rev. Lett*. **101,** 203901 (2008).

12. Liu, R., Ji, C., Mock, J. J., Chin, J. Y., Cui, T. J. & Smith, D. R., Broadband Ground-plane cloak. *Science* **323,** 366-369 (2009).

13. Valentine, J., Li, J., Zentgraf, T., Bartal G. & Zhang, X., An optical cloak made of dielectrics. *Nat.Mater*. **8,** 568 (2009).

14. Ma, H. F. & Cui, T. J., Three-dimensional broadband ground-plane cloak made of metamaterials. *Nat. Commun*. **1,** 21 (2010).

15. Ergin, T., Stenger, N., Brenner, P., Pendry, J. B. & Wegener, M., Three-dimensional invisibility cloak at optical wavelengths. *Science* **328,** 337 (2010).

16. Zhang, B., Chan, T. & Wu, B. Lateral shift makes a ground-plane cloak detectable. *Phys. Rev. Lett*. 104, 233903 (2010).

17. Zhang, B., Luo, Y., Liu, X. & Barbastathis, G. Macroscopic invisibility cloak for visible light. *Phys. Rev. Lett*. 106, 033901 (2011).

18. Chen, X. *et al*., Macroscopic invisibility cloaking of visible light. *Nat. Commun*. **2,** 176 (2011).

19. Kundtz, N. & Smith, D. R., Extreme-angle broadband metamaterial lens. *Nat. Mater*. **9,** 129 (2010).

20. Ma, H. F. & Cui, T. J., Three-dimensional broadband and broad-angle transformation-optics lens. *Nat. Commun.* **1,** 24 (2010).

21. Lai, Y. *et al*., Illusion optics: the optical transformation of an object into another object. *Phys. Rev. Lett*. **102,** 253902 (2009).

22. Jiang, W. X., Cui, T. J., Ma, H. F., Yang, X. M. & Cheng, Q., Shrinking an arbitrary object as one desires using metamaterials. *Appl. Phys. Lett*. **98,** 204101 (2011).

23. Zentgraf, T., Valentine, J., Tapia, N., Li J. & Zhang, X., An optical "Janus" device for integrated photonics. *Adv. Mater.* **22,** 2561 (2010).

24. Yu, N. *et al*., Light propagation with phase discontinuities: generalized laws of reflection and refraction. *Science* **334,** 333 (2011).

25. Engheta, N., Antenna-guided light. *Science* **334,** 317 (2011).

26. Ni, X. *et al*., Broadband light bending with plasmonic nanoantennas. *Science* **335,** 427 (2012).

27. Yin, X., Ye, Z., Rho, J., Wang, Y. & Zhang, X., Photonic spin hall effect at metasurfaces. *Science* **339,** 1405 (2013).

28. Lin, J. *et al*., Polarizaion-controlled tunable directional coupling of surface plasmon polaritons. *Science* **340,** 331 (2013).

29. Miroshnichenko, A. E. & Kivshar, Y. S., Polarization traffic control for surface plasmons. *Science* **340,** 283 (2013).

30. Grady, N. K. *et al*., Terahertz metamaterials for linear polarization conversion and anomalous refraction. *Science* **340,** 1304 (2013).

31. Chen, X. *et al*., Dual-polarity plasmonic metalens for visible light, *Nat. Commun*. **3,** 1198 (2012).

32. Sun, S. *et al*., Gradient-index meta-surface as a bridge linking propagating waves and surface waves. *Nat. Mater*. **11,** 426 (2012).

33. Sun, S. *et al*., High-efficiency broadband anomalous reflection by gradient metasurfaces. *Nano. Lett*. **12,** 6223 (2012).

34. Sersic, I., Tuambilangana, C., Kampfrath, T. & Koenderink, A. F. Magnetoelectric point scattering theory for metamaterial scatters. *Phy. Rev. B*. **83**, 245102 (2011).

35. Shmonina, E., Kalinin, V. A., Ringhofer, K. H. & Solymar, L. Magnetoinductive waves in one, two, and three dimensions. *J. Appl. Phys.* **92**, 6252 (2002).

36. Kwon, D.-H. & Werner, D. H. Polarization splitter and polarization rotator designs based on transformation optics. *Opt. Express* **16**, 18731 (2008).

37. Danner, A. J., Tyc, T. & Leonhardt, U. Controlling birefringence in dielectrics. *Nat. Photon.* 5, 357 (2011).

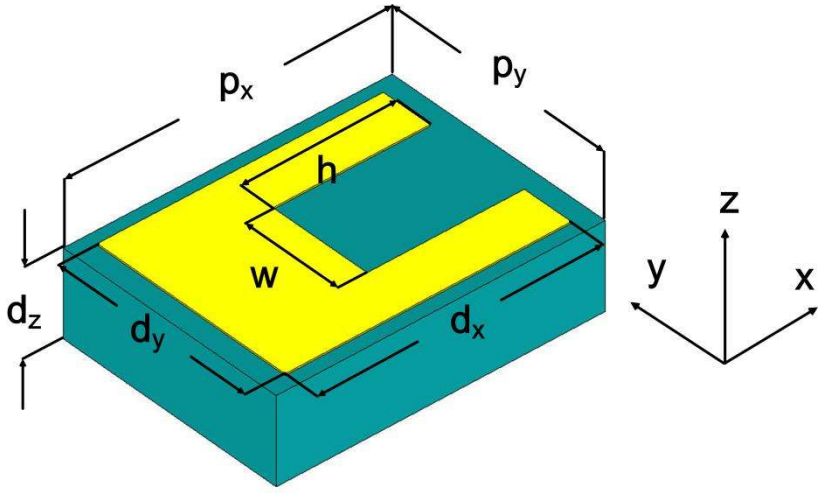

Figure 1. The proposed U-shaped structure and its detailed geometric parameters: p_x=4.6 mm, p_y=3.4 mm, d_x=4 mm, d_y=3 mm, d_z =1 mm, w=1.5 mm, and h spans from 1 mm to 3.4 mm with a step of 0.3 mm. The dielectric constant of the supporting slab is 2.2.

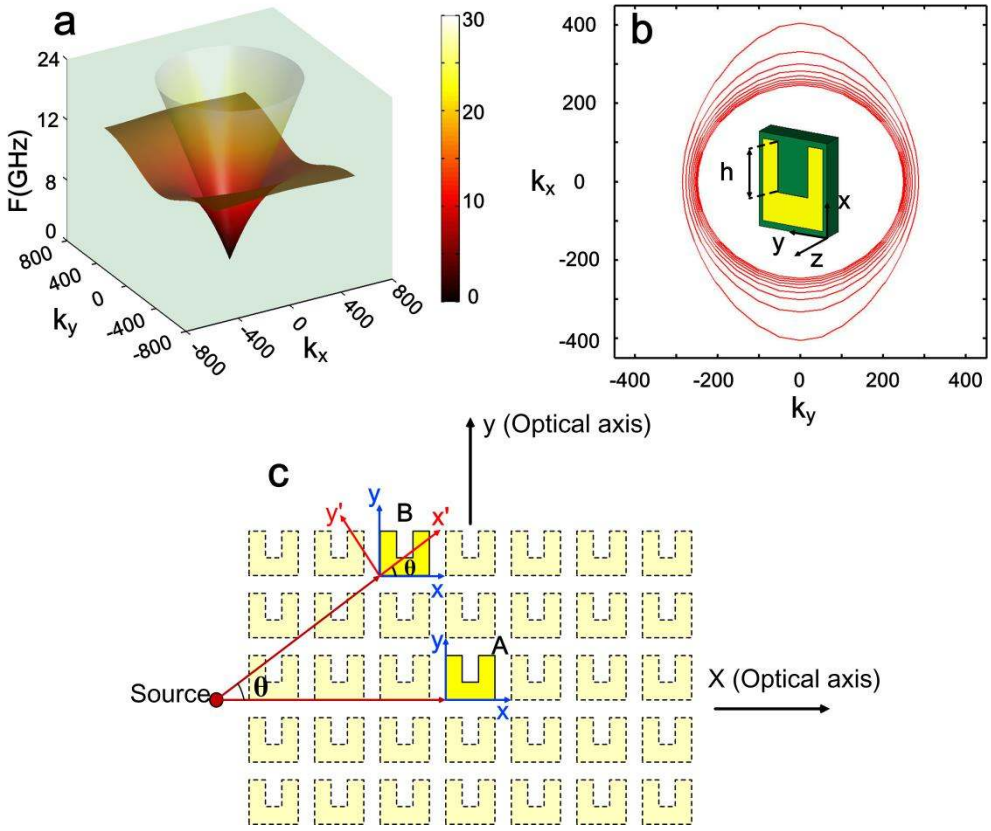

Figure 2. (a) The 2D dispersion surface of the U-shaped metallic structure on a dielectric support, in which p_x=4.6 mm, p_y=3.4 mm, d_x=4 mm, d_y=3 mm, d_z=1 mm, w=1.5 mm, h=2.2 mm, and the relative permittivity of the dielectric slab is 2.2, respectively. (b) The iso-frequency curves of the U-shaped particles at 10 GHz when the groove depth h increases from 1 mm (the innermost curve) to 3.4 mm (the outmost curve) with a step of 0.3 mm. The inset is a schematic of the U-shaped particle, in which the thickness of the metallic structure is 0.018 mm. It is observed that the anisotropy becomes weaker when the groove depth decreases until isotropy at h=1 mm. (c) A 2D array of the U-shaped particles (the shown case is homogeneous; it can also be inhomogeneous), in which x and y are two optical axes, and a point source is located on the horizontal optical axis. The rays emitting from the point source (red arrows) have different angles to different particles.

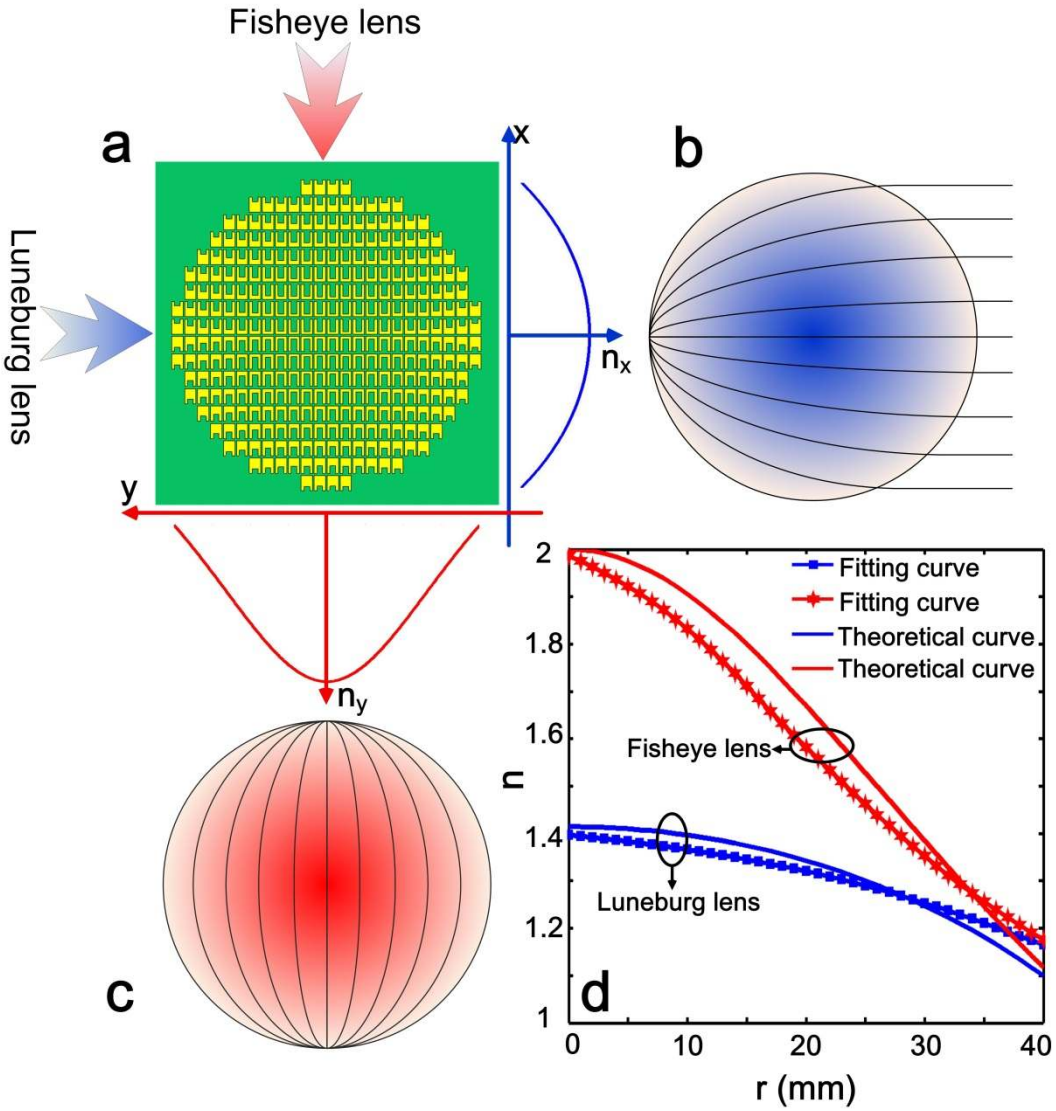

Figure 3. (a) Schematic diagram of the designed anisotropic metasurface lens, in which the big blue and red arrows indicate the directions of two optical axes. (b) Ray tracing of the anisotropic metasurface lens with n_x satisfying the ideal Luneburg distribution when the source is on the horizontal optical axis. Watching from the horizontal optical axis, the metasurface is a Luneburg lens. (c) Ray tracing of the anisotropic metasurface lens with n_y satisfying the ideal fisheye distribution when the source is on the vertical optical axis. Watching from the vertical optical axis, the metasurface is a fisheye lens. (d) Comparison between the ideal surface indexes of refraction for Luneburg and fisheye lenses and the effective indexes of refraction (n_x and n_y) for the realistic metasurface lens.

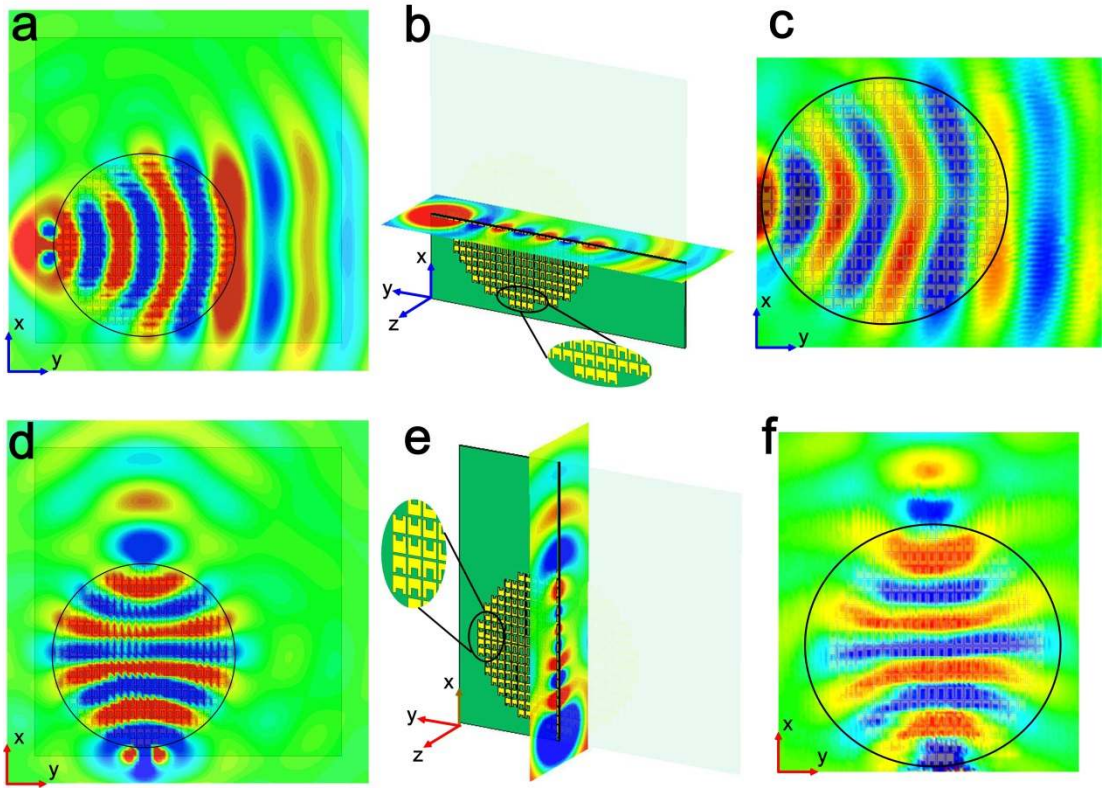

Figure 4. (a,c) Full-wave simulation and measured results of the electric-field (E_x) distributions on an observation plane that is 1 mm above the metasurface when the electric dipole is on the horizontal optical axis. (b) The simulated E_x distribution on a vertical observation plane passing through the horizontal optical axis, showing the surface wave nature inside the metalens. (d,f) Full-wave simulation and measured results of the E_x distributions on the observation plane that is 1 mm above the metasurface. (b) The simulated E_x distribution on a vertical observation plane passing through the vertical optical axis.

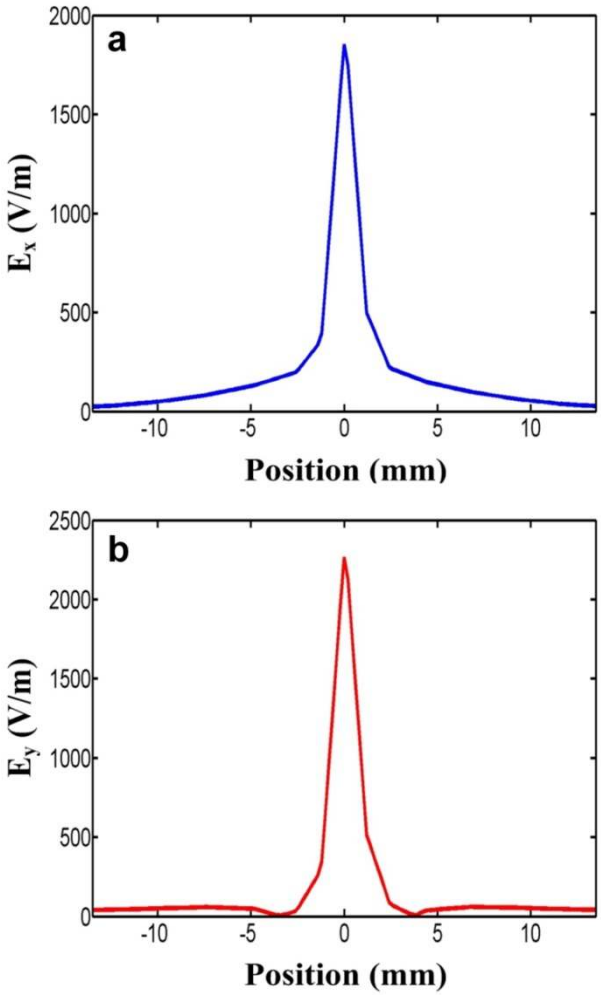

Figure 5. The field distributions along the *z* direction (i.e., perpendicular to the metasurface). (a) On the horizontal optical axis (Luneburg lens). (b) On the vertical optical axis (fisheye lens). We remark that the field distributions are not ideally symmetrical because the existence of dielectric supporting slab, which is located between 0 and 1 mm along the *z* axis in above figures.

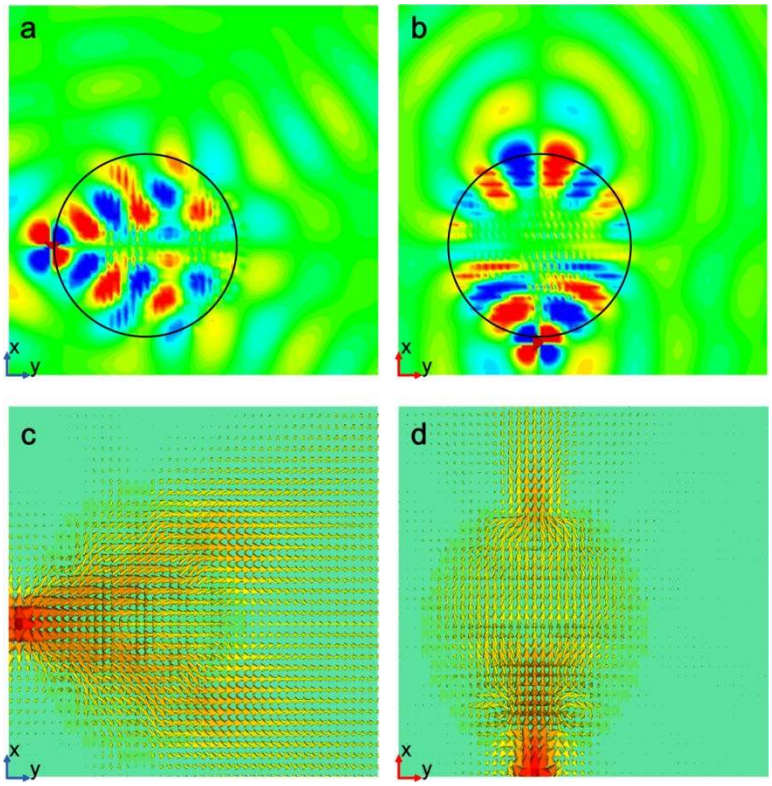

Figure 6. The simulated results of cross-polarized electric field distributions. (a) The E_y component of the Luneburg lens. (b) The E_x component of the Maxwell fisheye lens. (c) The power density when exciting along the y direction (the Luneburg lens). (d) The power density when exciting along the x direction (the fisheye lens)

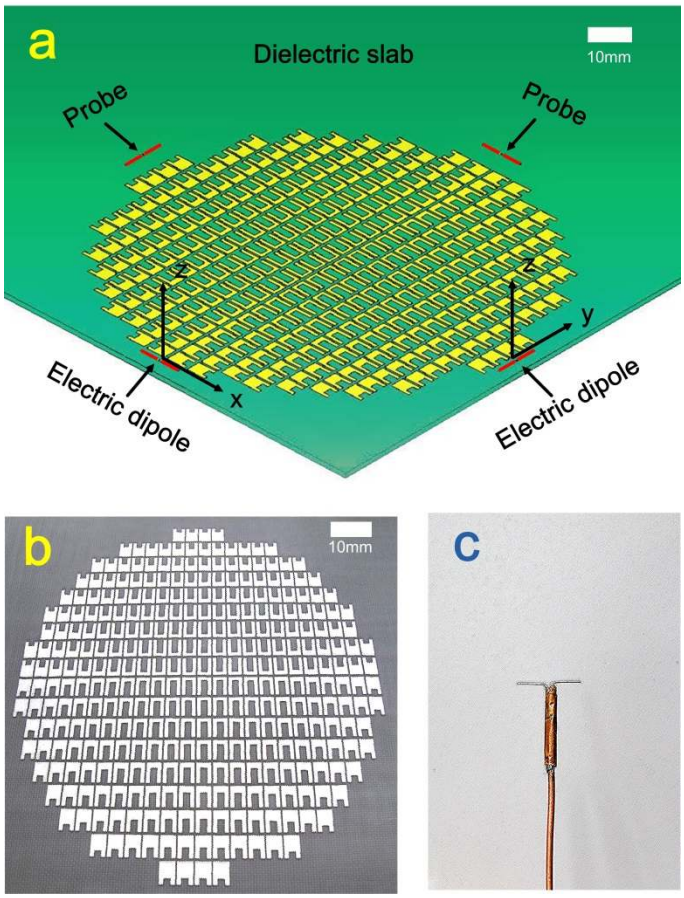

Figure 7. (a) The schematic configurations for simulations and measurements, including the metasurface lens and excitation and detection electric dipoles. The radius of the metasurface lens is 40mm. (b) A photo of the fabricated bi-functional anisotropic metalens. (c) A photo of the electric dipole for excitation and detection.

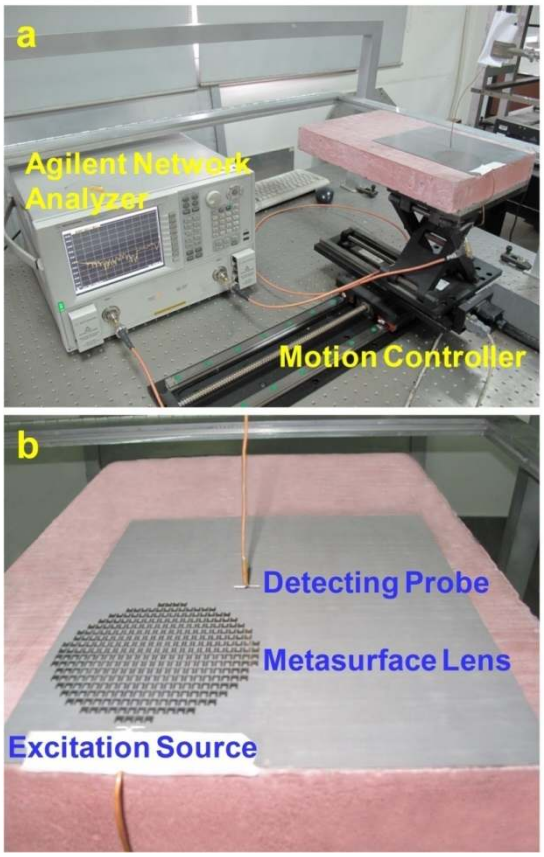

Figure 8. The experimental setup, including the measurement platform, fabricated sample, source and probing electric dipoles, and Agilent N5230C network analyzer. (a) An overview of the measurement setup. (b) Details of the testing sample, source, and detecting probe.